LETTERS

The structure of suspended graphene sheets

Jannik C. Meyer[1], A. K. Geim[2], M. I. Katsnelson[3], K. S. Novoselov[2], T. J. Booth[2] & S. Roth[1]

The recent discovery of graphene has sparked much interest, thus far focused on the peculiar electronic structure of this material, in which charge carriers mimic massless relativistic particles[1–3]. However, the physical structure of graphene—a single layer of carbon atoms densely packed in a honeycomb crystal lattice—is also puzzling. On the one hand, graphene appears to be a strictly two-dimensional material, exhibiting such a high crystal quality that electrons can travel submicrometre distances without scattering. On the other hand, perfect two-dimensional crystals cannot exist in the free state, according to both theory and experiment[4–9]. This incompatibility can be avoided by arguing that all the graphene structures studied so far were an integral part of larger three-dimensional structures, either supported by a bulk substrate or embedded in a three-dimensional matrix[1–3,9–12]. Here we report on individual graphene sheets freely suspended on a microfabricated scaffold in vacuum or air. These membranes are only one atom thick, yet they still display long-range crystalline order. However, our studies by transmission electron microscopy also reveal that these suspended graphene sheets are not perfectly flat: they exhibit intrinsic microscopic roughening such that the surface normal varies by several degrees and out-of-plane deformations reach 1 nm. The atomically thin single-crystal membranes offer ample scope for fundamental research and new technologies, whereas the observed corrugations in the third dimension may provide subtle reasons for the stability of two-dimensional crystals[13–15].

Whether a strictly two-dimensional (2D) crystal can exist was first raised theoretically more than 70 years ago by Peierls[4,5] and Landau[6,7]. They showed that, in the standard harmonic approximation[16], thermal fluctuations should destroy long-range order, resulting in melting of a 2D lattice at any finite temperature. Furthermore, Mermin and Wagner proved that a magnetic long-range order could not exist in one and two dimensions[17] and later extended the proof to crystalline order in 2D[8]. Importantly, numerous experiments on thin films have been in accord with the theory, showing that below a certain thickness, typically of dozens of atomic layers, the films become thermodynamically unstable (segregate into islands or decompose) unless they constitute an inherent part of a three-dimensional (3D) system (such as being grown on top of a bulk crystal with a matching lattice)[18–20]. However, although the theory does not allow perfect crystals in 2D space, it does not forbid nearly perfect 2D crystals in 3D space. Indeed, a detailed analysis of the 2D crystal problem beyond the harmonic approximation has led to the conclusion[13–15] that the interaction between bending and stretching long-wavelength phonons could in principle stabilize atomically thin membranes through their deformation in the third dimension[15]. Indeed, the experiments described here show that freely suspended graphene crystals can exist without a substrate, and exhibit random elastic deformations involving all three dimensions.

The preparation of graphene membranes used in this study is described in the text of the Supplementary Information and in Supplementary Fig. 1. Briefly, we used the established procedures[9] of micromechanical cleavage and identification of graphene, followed by electron-beam lithography and a number of etching steps, to obtain graphene crystallites attached to a micrometre-sized metallic scaffold. Figure 1 shows the bright-field transmission electron microscopy (TEM) image of one of our samples. The central parts of the prepared membranes normally appear on TEM images as homogeneous and featureless regions, whereas the membranes' edges tend to scroll (Fig. 1). Also, we often observed folded regions in which a graphene sheet became partly detached from the scaffold during microfabrication (right side of Fig. 1). Such folds provide a clear TEM signature for the number of graphene layers. A folded graphene sheet is locally parallel to the electron beam and, for monolayer graphene, a fold exhibits only one dark line (Fig. 2a), similar to TEM images from one-half of a single-walled carbon nanotube. For comparison, Fig. 2b shows a folded edge of bilayer graphene, which exhibits two dark lines, as in the case of double-walled nanotubes. One has to be careful, however, because scrolls and multiple folds can give rise to any number of dark lines even for monolayer graphene, as indeed observed experimentally.

In addition, we could directly distinguish between monolayer graphene and thicker samples by analysing nanobeam electron diffraction patterns from their flat areas as a function of incidence angle. This procedure effectively allowed us to probe the whole 3D reciprocal space. Figure 2 shows examples of diffraction patterns at three tilt angles for the graphene membrane of Fig. 1. As expected, there are

Figure 1 | Suspended graphene membrane. Bright-field TEM image of a suspended graphene membrane. Its central part (homogeneous and featureless region indicated by arrows) is monolayer graphene. Electron diffraction images from different areas of the flake show that it is a single crystal without domains. We note scrolled top and bottom edges and a strongly folded region on the right. Scale bar, 500 nm.

[1]Max Planck Institute for Solid State Research, Heisenbergstrasse 1, 70569 Stuttgart, Germany. [2]Manchester Centre for Mesoscience and Nanotechnology, University of Manchester, Oxford Road, Manchester M13 9PL, UK. [3]Institute for Molecules and Materials, Radboud University of Nijmegen, Toernooiveld 1, 6525 ED Nijmegen, The Netherlands.

two dominant reflections corresponding to periodicities of 2.13 and 1.23 Å, and weak higher-order peaks. The key for the identification of monolayer graphene is that its reciprocal space (Fig. 3) has only the zero-order Laue zone and, therefore, no dimming of the diffraction peaks should occur at any angle, in contrast to the behaviour of crystal lattices extended in the third dimension. This is exactly the behaviour we observed experimentally. Figure 2f plots the total intensity for diffraction peaks (0–110) and (1–210) as a function of tilt angle for monolayer graphene. One can see that changes in the
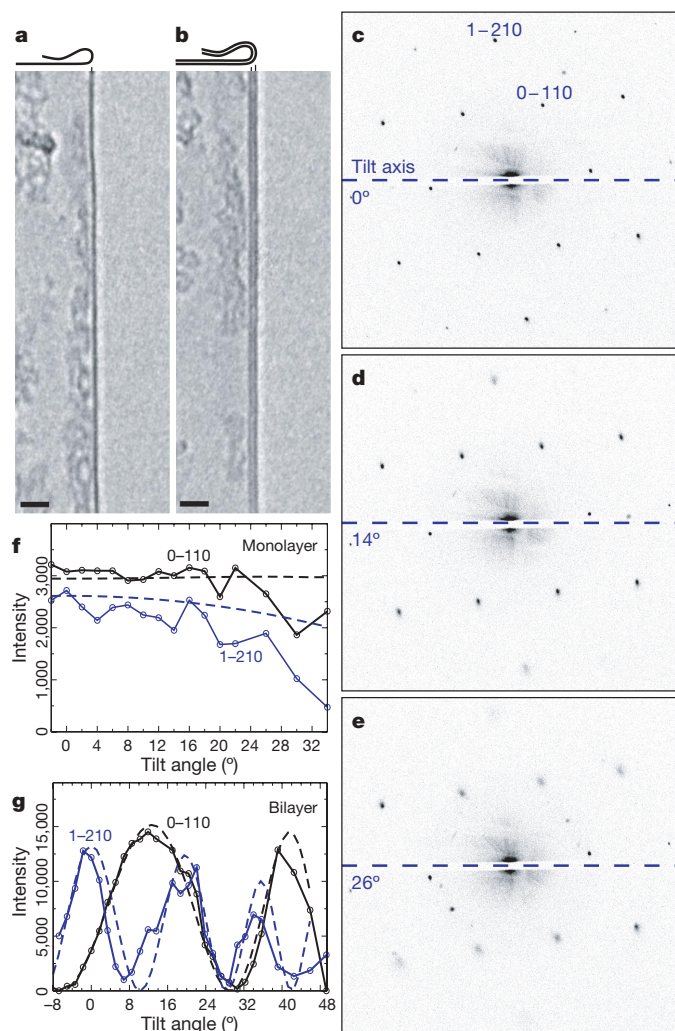
total intensity are relatively small and, importantly, there are no minima, in agreement with our numerical simulations (see Fig. 2 legend). For comparison, Fig. 2g shows the corresponding behaviour for bilayer graphene, where the total intensities vary so strongly that the same peaks become completely suppressed at some angles and the underlying sixfold symmetry remains undisturbed only for normal incidence. The diffraction analysis also shows that our bilayer membranes retained the Bernal (AB) stacking of bulk graphite, in contrast to the AAA... stacking reported in "carbon nanofilms"[21]. Independently of stacking order, the weak monotonic variation of diffraction intensities with tilt angle is a signature specific to monolayer graphene and can be used for its unambiguous identification in TEM.

Notwithstanding the overall agreement, there is one feature in the observed diffraction patterns that strongly disagrees with our numerical simulations and, more generally, with the standard diffraction behaviour in 3D crystals[22,23]. We can clearly see that the diffraction peaks in Fig. 2 become broader with increasing tilt angle and this

Figure 2 | Transmission electron microscopy of graphene. a, b, TEM images of folded edges for monolayer and bilayer graphene, respectively, using a Philips CM200 TEM. Scale bars, 2 nm. **c–e**, Electron diffraction patterns from a graphene monolayer under incidence angles of 0°, 14° and 26°, respectively. The tilt axis is horizontal. Here we used a Zeiss 912 TEM operated at 60 kV in the Köhler condition with the smallest (5 μm) condenser aperture. This allowed us to obtain a small, almost parallel beam with an illumination angle of 0.16 mrad and an illumination area of only 250 nm in diameter. The diffraction patterns were recorded on a charge-coupled device (CCD) for further quantitative analysis. The peaks become broader with increasing tilt, and this effect is strongest for peaks further away from the tilt axis. To label equivalent Bragg reflections, we use the Miller–Bravais indices (*hkil*) for graphite so that the innermost hexagon and the next one correspond to indices (0–110) (2.13 Å spacing) and (1–210) (1.23 Å spacing), respectively. **f**, Total intensity as a function of tilt angle for the peaks marked in **c**. To find the intensity values, each of the above Bragg reflections was fitted by a gaussian distribution for every angle, which yielded the peaks' intensities, positions, heights and widths. The dashed lines are numerical simulations, in which we used a Fourier transform of the projected atomic potentials[22,23,24] and the atomic form factors reported in ref. 29. **g**, The same analysis and simulations for a bilayer graphene membrane.
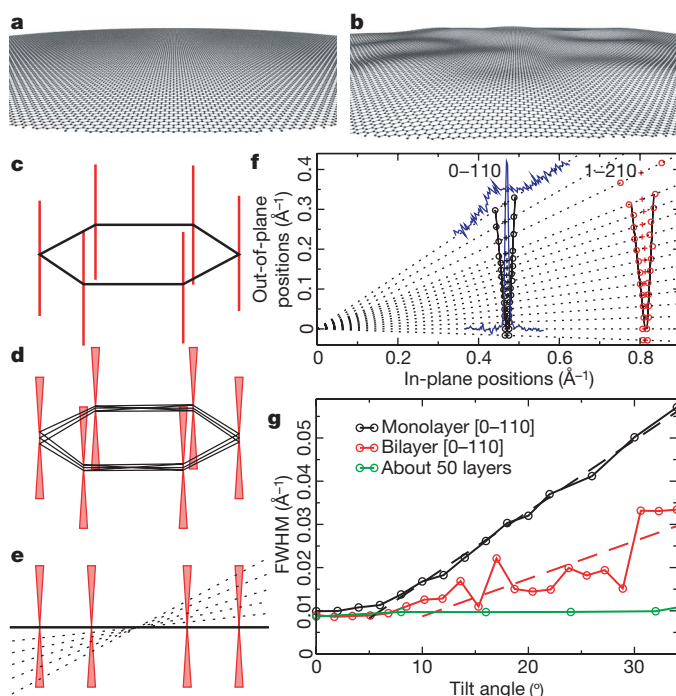
Figure 3 | Microscopically corrugated graphene. a, Flat graphene crystal in real space (perspective view). **b**, The same for corrugated graphene. The roughness shown imitates quantitatively the roughness found experimentally. **c**, The reciprocal space for a flat sheet is a set of rods (red) directed perpendicular to the reciprocal lattice of graphene (black hexagon). **d**, **e**, For the corrugated sheet, a superposition of the diffracting beams from microscopic flat areas effectively turns the rods into cone-shaped volumes so that diffraction spots become blurred at large angles (indicated by the dotted lines in **e**) and the effect is more pronounced further away from the tilt axis (compare with Fig. 2). Diffraction patterns obtained at different tilt angles allow us to measure graphene roughness. **f**, Evolution of diffraction peaks with tilt angle in monolayer graphene. The experimental data are presented in such a way that they closely resemble the schematic view in **e**. For each tilt angle, the black dotted line represents a cross-section for diffraction peaks (0–110) and (1–210). The peak centres and full widths at half maxima (FWHM) in reciprocal space are marked by crosses and open circles, respectively. In two cases (0° and 34°), the recorded intensities are shown in full by blue curves. All the intensity curves could be well fitted by the gaussian shape. The solid black lines show that the width of the diffraction spots reproduces the conical broadening suggested by our model (**d** and **e**). **g**, FWHM for the (0–110) diffraction peak in monolayer and bilayer membranes and thin graphite (as a reference), as a function of tilt angle. The dashed lines are the linear fits yielding the average roughness. The flat region between 0° to 5°, and also for the reference sample, is due to the intrinsic peak width for the microscope at our settings.

blurring is much stronger for those peaks that are further away from the tilt axis. This broadening is a distinctive feature of monolayer graphene. It becomes notably weaker in bilayer samples and completely disappears for multilayer graphene. From a theory point of view, the broadening is completely unexpected. To emphasize this, we note that, for example, thermal vibrations can only reduce the intensity of diffraction peaks (Debye–Waller factor) but do not lead to their broadening[22,24].

Figure 3 explains how the observed broadening explicitly reveals that graphene sheets are not flat within the submicrometre area of the electron beam. The full 3D Fourier transform of a flat graphene crystal (Fig. 3a) consists of a set of rods perpendicular to the plane of the reciprocal hexagonal lattice (Fig. 3c). Each diffraction pattern is then a two-dimensional slice (given by a section of the Ewald sphere) through this 3D space. In particular, this picture suggests that the intensity of diffraction peaks should vary without any singularities (monotonically) with changing tilt angle and the hexagonal symmetry is preserved for any tilt, as already discussed above. The increasing broadening of diffraction peaks without changes in their total intensity implies that the rods wander around their average direction (see Fig. 3d). This corresponds to a slightly uneven sheet (Fig. 3b) so that the diffraction pattern effectively comes from an ensemble of small flat 2D crystallites with different orientations with respect to the average plane. Figure 3e illustrates that such roughness results in sharp diffraction peaks for normal incidence, but that the peaks rapidly become wider with increasing tilt angle. This model also shows that their total intensity should be practically independent of the membrane's roughness and can be described by the angle dependence for a flat sheet; this is consistent with our simulations in Fig. 2f.

For quantitative analysis, Fig. 3f and g shows the detailed evolution of the broadening of the diffraction peaks with changing incidence angle. One can see that the peak widths increase linearly with tilt and also proportionally to the peaks' position in reciprocal space, in quantitative agreement with our simulations for corrugated graphene. The width of the cones or the linear slopes in Fig. 3f and g provide a direct measure of the membrane's roughness. For different monolayer membranes, we found cone angles between $8°$ and $11°$, that is, the surface normal deviated from its mean direction on average by $\pm 5°$. For bilayer membranes, this value was found to be about $2°$ (Fig. 3g). We note that the diffraction peaks broaden isotropically (see Fig. 2c–e). This means that the surface normal in real space wanders in all directions, and the observed waviness is omni-directional. Otherwise, if a graphene membrane were curved only in one direction, diffraction peaks would spread into a line indicating the direction of curling. An absolutely incompressible sheet can only be curved in one direction, not two, and the isotropic waviness unambiguously implies local deformations of graphene. The curvature of $5°$ yields a local strain of up to 1%, which is large but sustainable without plastic deformation and generation of defects[25–27].

To estimate the spatial extent L of the corrugations we found, let us start with two observations. First, L cannot be drastically (more than a few times) smaller than the coherence length of the diffracted electrons. Otherwise, the above model of incoherent superpositions from locally flat pieces would be replaced by a coherent superposition where we would expect sharp peaks and also much stronger deviations between the experimental and calculated intensities in Fig. 2f. The coherence length is estimated to be about 10 nm, so the corrugations must have a mesoscopic (several nanometres) rather than atomic scale. Second, the smooth gaussian shape of the diffraction peaks requires a large number N of different orientations within the submicrometre illuminated area, which provides us with the upper limit for L. A minimalist assumption of $N = 100$ necessitates $L \leq 25$ nm. These qualitative considerations are in agreement with our simulated diffraction patterns for corrugated graphene sheets (see text on numerical simulations in the Supplementary Information and Supplementary Figs 2–5). From the known curvature

and size L of the corrugations, we estimate their height to be about 1 nm.

The above order-of-magnitude estimates are also strongly supported by atomic-resolution TEM imaging of our membranes. Unfortunately, for monolayer graphene, such smooth waviness could not be visualized because diffraction intensities vary little with tilt angle, as discussed earlier (Fig. 2f), and no additional contrast due to corrugations could be expected or, in fact, observed. On the other hand, the visibility of the hexagonal lattice for two and more layers strongly depends on their tilt angle (Fig. 2g) and, accordingly, surface undulations of few-layer graphene can be expected to result in areas of different brightness. Such areas are clearly seen in Fig. 4 and have a characteristic size of a few nanometres, which is somewhat smaller than the above estimate for L in monolayer graphene where the ripples could also be larger laterally. Importantly, atomic-resolution images show that the corrugations are static, because otherwise, changes during the exposure would lead to blurring and disappearance of the additional contrast.

Perfect 2D atomic crystals cannot exist, unless they are of a limited size or contain many crystal defects[7,8]. The observed microscopic corrugations of 2D graphene in the third dimension provide another, unexpected way to reconcile the high quality of graphene with its thermodynamic stability. The fact that the microscopic roughness is reproducible for different positions on membranes and for different samples, becomes notably smaller for bilayer graphene and disappears for thicker membranes proves that the corrugations are intrinsic to graphene membranes. Theoretical investigations of 2D membranes have predicted their thermodynamic stability through static microscopic crumpling involving either bending or buckling[13–15]. The buckling mechanism requires the generation of a high density of dislocations[15] that are neither observed in our atomic-resolution images nor expected in the case of relatively small (micrometre-sized) membranes with strong interatomic bonds. However, the bending scenario assumes no defects and only requires out-of-plane deformations involving a significant elastic strain. The latter is in qualitative agreement with our observations, but further experimental and theoretical studies are needed to clarify the detailed mechanism of the corrugations in graphene.

Free-hanging graphene is the thinnest conceivable object and thus offers many exciting directions for future research. The observed
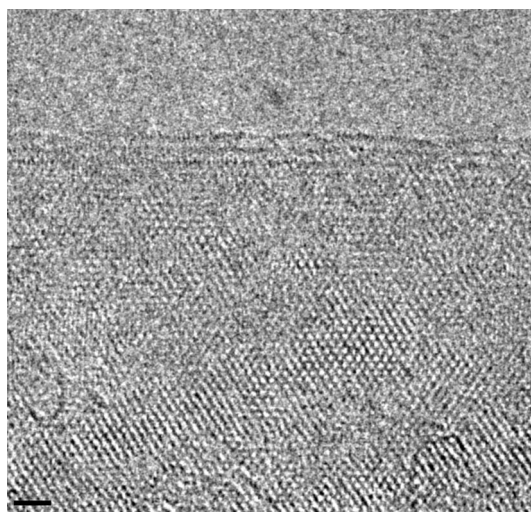

Figure 4 | Atomic resolution imaging of graphene membranes. TEM image of a few-layer graphene membrane near its edge, where the number of dark lines indicates the thickness of two to four layers. Because for few-layer graphene the electron contrast depends strongly on incidence angle, relatively small (a few degrees) variations in the surface normal become visible. The atomic-resolution imaging was achieved by using FEI Titan at an acceleration voltage of 300 kV. Scale bar, 1 nm.

microscopic roughening seems to be essential for the structural stability of 2D membranes; their mechanical, electronic, optical and other properties may be equally extraordinary. We also note that the presence of these elastic corrugations is consistent with high mobility of charge carriers in graphene[1–3] and may explain some of its unusual transport characteristics, such as the suppression of weak localization[28]. 2D crystal membranes also promise such tantalizing applications as almost-transparent substrates for high-resolution electron microscopy or sieving of atoms and small molecules through the atomic-size benzene rings. Such 2D membranes can be considered for any other technology in which ultrathin, transparent and robust substrates offer an advantage (for example, nanomechanical devices).

1. Novoselov, K. S. *et al.* Electric field effect in atomically thin carbon films. *Science* **306**, 666–669 (2004).
2. Novoselov, K. S. *et al.* Two-dimensional gas of massless Dirac fermions in graphene. *Nature* **438**, 197–200 (2005).
3. Zhang, Y., Tan, J. W., Stormer, H. L. & Kim, P. Experimental observation of the quantum Hall effect and Berry's phase in graphene. *Nature* **438**, 201–204 (2005).
4. Peierls, R. E. Bemerkungen über Umwandlungstemperaturen. *Helv. Phys. Acta* **7**, 81–83 (1934).
5. Peierls, R. E. Quelques proprietes typiques des corpses solides. *Ann. Inst. Henri Poincare* **5**, 177–222 (1935).
6. Landau, L. D. Zur Theorie der Phasenumwandlungen II. *Phys. Z. Sowjetunion* **11**, 26–35 (1937).
7. Landau, L. D. & Lifshitz, E. M. S*tatistical Physics* Part I, Sections 137 and 138 (Pergamon, Oxford, 1980).
8. Mermin, N. D. Crystalline order in two dimensions. *Phys. Rev.* **176**, 250–254 (1968).
9. Novoselov, K. S. *et al.* Two-dimensional atomic crystals. *Proc. Natl Acad. Sci. USA* **102**, 10451–10453 (2005).
10. Berger, C. *et al.* Electronic confinement and coherence in patterned epitaxial graphene. *Science* **312**, 1191–1196 (2006).
11. Ohta, T., Bostwick, A., Seyller, T., Horn, K. & Rotenberg, E. Controlling the electronic structure of bilayer graphene. *Science* **313**, 951–954 (2006).
12. Stankovich, S. *et al.* Graphene-based composite materials. *Nature* **442**, 282–286 (2006).
13. Nelson, D. R. & Peliti, L. Fluctuations in membranes with crystalline and hexatic order. *J. Phys.* **48**, 1085–1092 (1987).
14. Radzihovsky, L. & Le Doussal, P. Self-consistent theory of polymerized membranes. *Phys. Rev. Lett.* **69**, 1209–1212 (1992).
15. Nelson, D. R., Piran, T. & Weinberg, S. *Statistical Mechanics of Membranes and Surfaces* (World Scientific, Singapore, 2004).
16. Born, M. & Huang, K. *Dynamical Theory of Crystal Lattices* (Clarendon, Oxford, 1954).
17. Mermin, N. D. & Wagner, H. Absence of ferromagnetism or antiferromagnetism in one- or two-dimensional isotropic Heisenberg models. *Phys. Rev. Lett.* **17**, 1133–1136 (1966).
18. Venables, J. A., Spiller, G. D. T. & Hanbucken, M. Nucleation and growth of thin-films. *Rep. Prog. Phys.* **47**, 399–459 (1984).
19. Zinkeallmang, M., Feldman, L. C. & Grabow, M. H. Clustering on surfaces. *Surf. Sci. Rep.* **16**, 377–463 (1992).
20. Evans, J. W., Thiel, P. A. & Bartelt, M. C. Morphological evolution during epitaxial thin film growth: Formation of 2D islands and 3D mounds. *Surf. Sci. Rep.* **61**, 1–128 (2006).
21. Horiuchi, S. *et al.* Carbon nanofilm with a new structure and property. *Jpn. J. Appl. Phys.* **42**, L1073–L1076 (2003).
22. Buseck, P. R., Cowley, J. M. & Eyring, L. *High-Resolution Transmission Electron Microscopy* (Oxford Univ. Press, Oxford, 1988).
23. Spence, J. C. H. *High-Resolution Electron Microscopy* (Oxford Univ. Press, Oxford, 2003).
24. Peng, L. M. Electron atomic scattering factors and scattering potentials of crystals. *Micron* **30**, 625–648 (1999).
25. Yu, M. F., Files, B. S., Arepalli, S. & Ruoff, R. S. Tensile loading of ropes of single wall carbon nanotubes and their mechanical properties. *Phys. Rev. Lett.* **84**, 5552–5555 (2000).
26. Zhao, Q., Nardelli, M. B. & Bernholc, J. Ultimate strength of carbon nanotubes: a theoretical study. *Phys. Rev. B* **65**, 144105 (2002).
27. Huang, J. Y. *et al.* Superplastic carbon nanotubes. *Nature* **439**, 281 (2006).
28. Morozov, S. V. *et al.* Strong suppression of weak localization in graphene. *Phys. Rev. Lett.* **97**, 016801 (2006).
29. Doyle, P. A. & Turner, P. S. Relativistic Hartree-Fock x-ray and electron scattering factors. *Acta Crystallogr. A* **24**, 390–397 (1968).

Author Information Reprints and permissions information is available at www.nature.com/reprints. The authors declare no competing financial interests. Correspondence and requests for materials should be addressed to J.C.M. (email@jannikmeyer.de) and A.K.G. (geim@man.ac.uk).